Quantum interference and electron interaction effects in CaAl(Au,Ag) amorphous alloys

1992 J. Phys.: Condens. Matter 4 9355

(http://iopscience.iop.org/0953-8984/4/47/016)

J. Phys.: Condens. Matter 4 (1992) 9355–9366. Printed in the UK

Quantum interference and electron interaction effects in CaAl(Au, Ag) amorphous alloys

F M Mayeya and M A Howson
Department of Physics, University of Leeds, Leeds LS2 9JT, UK

Received 30 July 1992

Abstract. We present magnetoconductivity results for a series of CaAl(Au) and CaAl(Ag) amorphous alloys. We have carried out a systematic study of the effect of varying the strength of the spin–orbit scattering in these alloys by introducing small concentrations of Au, Ag and Cu. The data are analysed using existing theories of quantum interference and electron interaction effects in disordered metals, from which estimates of the inelastic and spin–orbit scattering times have been obtained.

The inelastic scattering is largely unaffected by the heavy-element doping while the spin–orbit scattering rate systematically increases and saturates at about 3% Au with a value of 1×10^{12} s^{-1}. There is also a marked reduction in the contribution of electron interaction effects to the magnetoconductivity in the presence of strong spin–orbit scattering. Indeed the contribution is completely destroyed by as little as 1% Au.

1. Introduction

Theories of quantum interference effects (QIEs) and electron interaction effects (EIEs) have been used widely to describe the behaviour of the electrical conductivity in disordered metals [1–4]. Both these effects are quantum corrections to the usual semiclassical treatment of electron transport, arising from the structural disorder and strong elastic scattering in amorphous alloys. The propagation of conduction electrons is diffusive in nature because of the short elastic mean free path. Quantum interference refers to the interference of oppositely directed electron partial scattered waves traversing the same closed path. Coherent interference between the partial waves results and leads to a decrease in the electrical conductivity. The phase coherence can be destroyed by inelastic scattering, spin flip scattering or a magnetic field—characterized by the scattering rates τ_i^{-1}, τ_{sf}^{-1} and magnetic dephasing rate τ_b^{-1} respectively—and provides a natural explanation for the observed negative temperature coefficient of resistivity and the negative magnetoresistance reported in many high-resistivity disordered systems [1–4]. Spin–orbit scattering characterized by the scattering rate τ_{so}^{-1} has a very subtle effect on the QIE and gives rise to coherent interference which increases the conductivity—sometimes called a delocalizing effect. A clear explanation of this has been given by Dugdale [5].

The strength of the spin–orbit scattering greatly affects the magnetoconductivity. When the spin orbit scattering is strong ($\tau_{so}^{-1} > \tau_i^{-1}$) the magnetoconductivity is negative. When it is weak ($\tau_{so}^{-1} < \tau_i^{-1}$) the magnetoconductivity is positive, and for intermediate cases a change in sign is observed from negative in low fields

0953-8984/92/479355+12$07.50

($\tau_{so}^{-1} > \tau_b^{-1}$) to positive in high fields ($\tau_{so}^{-1} < \tau_b^{-1}$). The sign of the temperature coefficient of the conductivity also depends on the strength of the spin–orbit scattering in a similar way, namely when $\tau_{so}^{-1} > \tau_i^{-1}$, at low temperatures, the conductivity decreases with increasing temperature.

EIEs are related to QIEs but involve the interaction between two different electrons. This was explained in a simple physical way by Bergmann [6]. The first electron sets up a charge distribution through the QIE which Bergmann describes as a charge hologram. The second electron interacts with this charge distribution and is scattered. The scattering is unusual in that the scattering may enhance the conductivity. The effect requires phase coherence between the two interacting electrons and so is characterized by a phase coherence time related to the average energy separation of the interacting electrons. The effect is thus destroyed as the temperature is increased and the average energy separation increases as $k_B T$ or by the Zeeman splitting in a magnetic field where the energy separation is $g\mu_B B$. Inelastic scattering can also remove the effect by destroying the charge hologram set up by the quantum interference. We also see evidence for a reduction in the size of the effect in the presence of strong spin–orbit scattering.

In this work we have carried out a systematic study of the effect of spin–orbit scattering on QIEs and EIEs in the simple metal amorphous alloys, $Ca_{80}Al_{20}$ and $Ca_{60}Al_{40}$, by doping with the heavy elements Au, Ag and Cu. There have been a number of studies of spin–orbit scattering in amorphous alloys but they have concentrated on comparisons of different alloy systems. There has also been a study of the effects of Au doping in the MgCu system by Richter *et al* [4] although they found it difficult to fit the theory to their data for fields above about 2 Tesla—this may be because they were overestimating the contribution from the EIE.

We report here on a study of the effect in a simple metal system where the spin–orbit scattering is controlled by low levels of doping with a heavy element. We have chosen the composition $Ca_{80}Al_{20}$ since it has the lowest resistivity of the CaAl series ($\simeq 140\,\mu\Omega$ cm) and we are as close to the limit $k_F l \gg 1$ as we can get and still see QIEs clearly. We have also chosen to look at $Ca_{60}Al_{40}$ for comparison, since it has a much higher resistivity. There are a significant number of 'd' states at the Fermi energy coming from the tail of the Ca 'd' band [7]. These probably provide a source of strong s–d scattering which produces such a highly resistive alloy but there are not enough to produce a dominant contribution to the conduction. This is not the case in many of the other systems studied. For example the conduction in the CuZr and CuTi systems have been shown to be primarily due to 'd' band conduction with the 'd' electrons contributing as much as 80% to the conductivity [1].

2. Experimental techniques

The alloys were prepared using the melt-spinning technique. Components of the desired composition were prepared from Johnson Matthey resublimed calcium (99.5%), aluminium (99.999%), gold (99.9%) and silver (99.9%). The ingot was formed in an argon arc furnace. To ensure homogeneity each alloy was melted and turned many times. This process tended to lead to a small reduction in amount of the calcium in the final ingot. The alloys were then melt-spun in a chamber filled with helium gas at 0.1 mbar producing ribbons of typical thickness 20 to 30 μm, width 1 to 2 mm and length 200 to 500 mm. The resistance was measured using a standard four-probe DC technique with a precision of one part in 10^5. The magnetoconductivity was

measured in fields up to 7 Tesla at temperatures between 1.5 and 25 K. The chemical composition of the samples was obtained using inductively coupled plasma–atomic emission spectroscopy (ICP–AES) and also by electron microprobe analysis (EMA).

3. Theoretical review

The complete expression for the magnetoconductivity due to QIEs which includes inelastic and spin–orbit scattering, Zeeman splitting and orbital effects is given by Fukuyama and Hoshino [8] for a nonsuperconducting alloy as

$$\Delta\sigma(B,T) = A[\![b\{f_3[h/(1+t)] + c[f_3(h/t_+) - f_3(h/t_-)]\} + (1/D\tau_{SO})^{1/2}\{-[1/(1-\gamma)^{1/2}](t_-^{1/2} - t_+^{1/2}) + t^{1/2} - (t+1)^{1/2}\}]\!] \quad (1)$$

where

$$t_\pm = t + 0.5[1 \pm (1-\gamma)^{1/2}]$$

$$A = e^2/2\pi^2\hbar \qquad b = (eB/\hbar)^{1/2} \qquad c = 0.5/(1-\gamma)^{1/2}$$

$$h = DeB\tau_{so}/\hbar \qquad \gamma = [g\mu_B B\tau_{SO}/2\hbar]^2 \qquad t = \tau_{so}/4\tau_i.$$

Baxter *et al* [9] have produced an analytic expression for $f_3(x)$. D is the diffusion constant which can be found from the Einstein relation $\sigma = e^2N(E_F)D$.

There are two contributions to the magnetoconductivity from the EIEs: a Zeeman splitting term [10] and an orbital term [11]. The orbital term makes only a very small contribution at the temperature and fields in this study and so is neglected. Lee and Ramakrishnan [10] found the Zeeman spin splitting term to be

$$\Delta\sigma(B) = -(e^2/4\pi^2\hbar)F_\sigma(k_BT/2\hbar D)^{1/2}G(T,B) \quad (2)$$

where

$$F_\sigma = -\tfrac{32}{3}[1 + 3F/4 - (1+F/2)^{3/2}]/F.$$

Here F is the electron–electron screening factor. Analytic expressions for $G(T,B)$ have been derived by Ousset *et al* [12]. In all these expressions the spin-flip scattering rate due to magnetic impurities has not been shown explicitly. As a result the values of the inelastic and spin–orbit scattering rates also include any spin-flip scattering. However in our case spin-flip scattering is small and can be largely neglected.

It is difficult to determine the spin-flip scattering rate due to magnetic impurities. However CaAl is a good system to work with since it has a low level of transition metal impurities. For example in our ICP–AES analysis, which has a detection limit of about 1 ppm, we could not detect the presence of Cr, Fe or Mn. In the magnetoresistance analysis the presence of magnetic impurities would lead to an apparent saturation of the inelastic scattering rate at low temperatures when determined by fitting equation (1) to the magnetoconductivity. Indeed we see some evidence of saturation in the inelastic scattering rate below 4 K which is consistent with magnetic impurities at the low level of about 1 ppm.

4. Results and discussion

In the analysis, the data were fitted to the QIE and EIE theoretical expressions given in equations (1) and (2) using a non-linear fitting routine and the analytic expressions as outlined by Baxter *et al* [9]. Only the Zeeman spin-splitting term of the EIE was included in the fit since the orbital term makes a negligible contribution in the temperature and field ranges of 1.5–25 K and 0–7 Tesla respectively in which the magnetoconductivity measurements were performed.

In fitting the data to theory, only two free parameters were used, the spin–orbit and inelastic scattering rates. The values of the diffusion constant, D, for $Ca_{80}Al_{20}$ and $Ca_{60}Al_{40}$ used in the fits were calculated from the measured conductivities and density of states deduced from specific heat measurements [13]—it is important to use the values of the specific heat enhanced by the electron–phonon mass enhancement. These values were kept constant for all the other samples doped with Au or Ag. This step was based on the assumption that the density of states ($N(E_F)$) at the Fermi level is not appreciably changed with the introduction of small concentrations of Au or Ag.

The screening parameter F was not used as a fitting parameter within the non-linear least square fitting routine, but was progressively varied for each sample until the best fit was obtained at all temperatures. F itself is independent of temperature.

Table 1 shows the values of various parameters deduced from the magnetoconductivity measurements. There is an error of about 20% in the electrical resistivity but the values are comparable with those of Howson *et al* [14] and Mizutani and Matsuda [13].

Table 1. Characteristic parameters of CaAl (Au, Ag) amorphous alloys.

Alloy	ρ ($\mu\Omega$ cm)	D (10^{-5} m^2 s^{-1})	F	τ_{so} (ps)	β (ns K^2)
$(Ca_{80}Al_{20})_{100-x}M_x$					
$x = 0$	167	9.6	0.25	33	1.6
M = Ag $x = 0.5$	130	9.6	0.23	22	1.2
$x = 2.5$	122	9.6	0.10	15	1.3
M = Au $x = 0.35$	133	9.6	0.10	5.8	1.5
$x = 1.3$	159	9.6	0.00	1.7	1.3
$x = 2.9$	133	9.6	0.00	1.0	1.6
$x = 5.8$	168	9.6	0.00	0.9	1.0
$(Ca_{60}Al_{40})_{100-x}Au_x$					
$x = 0$	330	6.7	0.10	73	2.0
$x = 0.2$	271	6.7	0.05	8.2	1.5
$x = 0.5$	310	6.7	0.05	1.9	1.6

Figures 1(*a*), (*b*), (*c*) and (*d*) show the field and temperature dependence of the magnetoconductivity of $(Ca_{80}Al_{20})_{100-x}$(Au, Ag)$_x$ for different strength of spin–orbit scattering. They illustrate the behaviour of the magnetoconductivity under weak, moderate and strong spin–orbit scattering. The points are experimental data while the solid lines are the theoretical fits to the data. Figure 1(*a*) shows the magnetoconductivity of $Ca_{80}Al_{20}$ alloy in which the spin–orbit scattering is very weak. The magnetoconductivity is positive except at very low fields ($B < 1$ T) where it is negative. At such low fields, the dephasing rate due to the magnetic field τ_b^{-1} is less

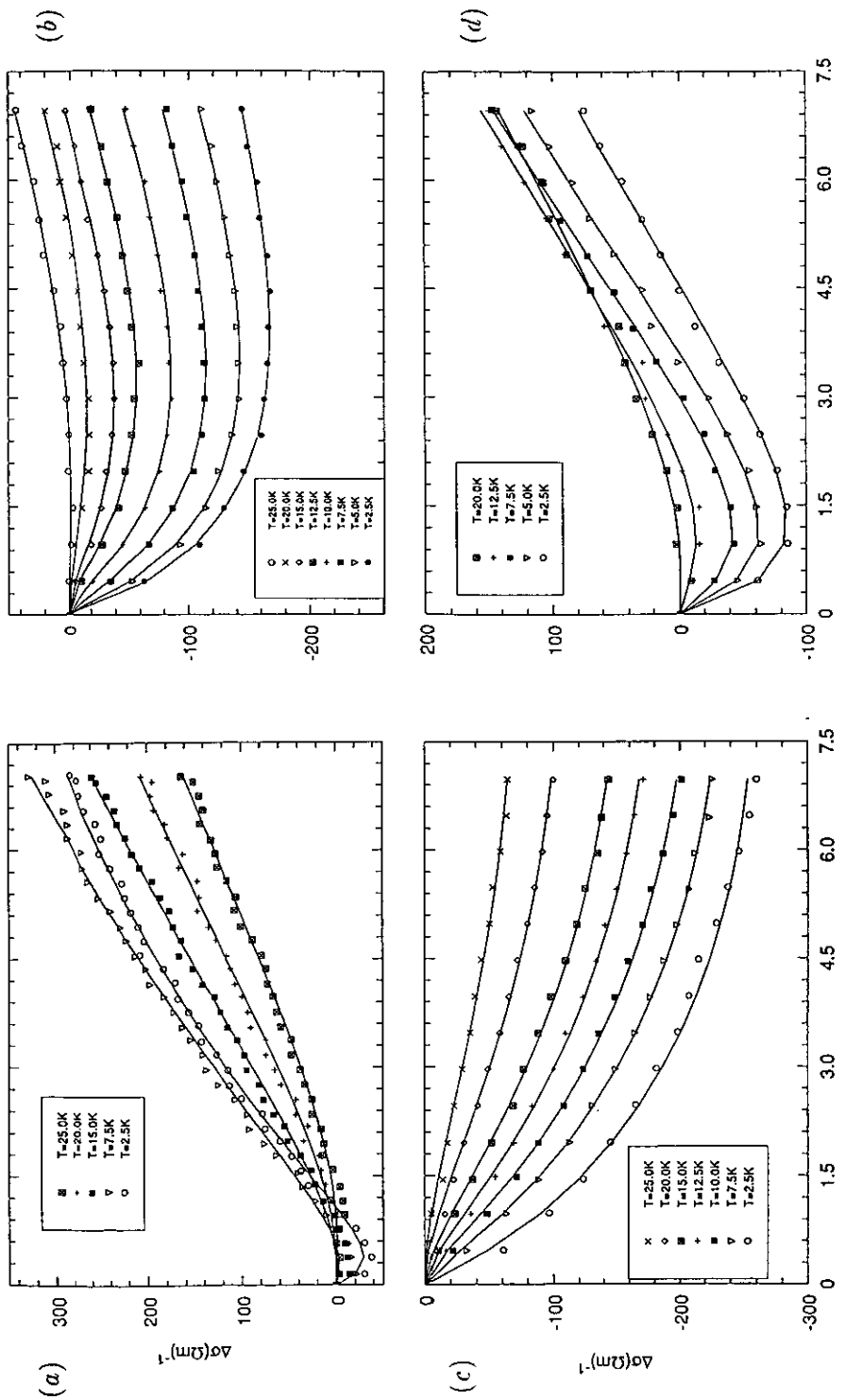

Figure 1. Magnetoconductivity of $(Ca_{80}Al_{20})_{100-x}Au_x$ at various temperatures for (*a*) $x = 0$, (*b*) $x = 0.35$, (*c*) $x = 1.34$ and for $(Ca_{80}Al_{20})_{100-x}Ag_x$ with (*d*) $x = 2.5$.

than the spin–orbit scattering rate τ_{so}^{-1} ($\tau_b^{-1} < \tau_{so}^{-1}$) and the spin–orbit interaction effect dominates producing the negative magnetoconductivity. When the magnetic field is increased beyond 1 T, the value of τ_b^{-1} exceeds that of τ_{so}^{-1} and the spin–orbit scattering effect is diminished resulting in positive magnetoconductivity. The value of τ_{so}^{-1} for this alloy was 3×10^{10} s^{-1}, contrary to the initial work of Howson *et al* [14] who obtained a value of $\simeq 10^4$ s^{-1}. This low value of Howson *et al* was a result of the fact that in their measurements the low-field negative magnetoconductivity, critical in the determination of τ_{so}, was not measured accurately and therefore their fit was not sensitive to the exact value of τ_{SO}.

In figure 1(*b*), the magnetoconductivity of $(Ca_{80}Al_{20})_{99.65}Au_{0.35}$ is shown. The change in sign of the magnetoconductivity from negative to positive takes place at a higher field ($\simeq$ 3.5 T) because of the increase in the spin–orbit scattering. In this alloy, the strength of the spin–orbit scattering is moderate. Figure 1(*c*) shows the magnetoconductivity of $(Ca_{80}Al_{20})_{98.66}Au_{1.34}$ representing a strong spin–orbit scattering alloy in which there is no change in sign of the magnetoconductivity. It is negative over the entire field range.

Figure 1(*d*) shows the magnetoconductivity of $(Ca_{80}Al_{20})_{97.5}Ag_{2.5}$. The strength of the spin–orbit scattering in this alloy is intermediate between the 0.0% and 0.35% Au alloys. This result reflects the fact that Au is a much stronger spin–orbit scatterer than Ag because Au is a heavier element. The addition of 1% Cu did not appreciably affect the magnetoconductivity of $Ca_{80}Al_{20}$. This indicates that it is a much weaker spin–orbit scatterer than the CaAl host.

It is clear from figures 1(*a–d*) that the magnetoconductivity is temperature dependent. Its magnitude decreases as the temperature is increased because of the increase in the electron–phonon inelastic scattering which destroys the phase coherence of the electron wave functions. The inelastic scattering rate (τ_i^{-1}) is less than the spin–orbit scattering rate for strong spin–orbit scattering and the magnetoconductivity is negative at all temperatures. In the case of weak or moderate spin–orbit scattering, $\tau_{so}^{-1} \leqslant \tau_i^{-1}$ and a change in sign of the magnetoconductivity occurs depending on the value of τ_b^{-1} relative to both τ_i^{-1} and τ_{so}^{-1}.

Figure 2 illustrates the temperature dependence of the inelastic scattering rate for three alloys with different strengths of spin–orbit scattering determined from the theoretical fit. They all exhibit the same temperature dependence of the form $\tau_I^{-1} = \tau_0^{-1} + T^2/\beta$. The value of β is independent of the Au or Ag concentration and has a value of $\simeq 1 \times 10^{-9}$ s K^2 as can be seen from table 1. At lower temperatures τ_i saturates to a constant value τ_0. This saturation is most probably due to the presence of magnetic impurities [4]. The level of magnetic impurities in our alloys is below 1 ppm (from ICP–AES analysis) and the saturation in the inelastic scattering time below 4 K indicates the presence of these impurities at very low concentrations. There is, in fact, a wide variation in the value of τ_0, which does not correlate with the Au and Ag doping concentration. This suggests that, despite careful handling of the samples during preparation, the main source of magnetic impurities comes from contamination during preparation, and not from the starting materials.

Figure 3 shows the comparison of the magnetoconductivity for alloys with different strengths of spin–orbit scattering at 18 K. In this figure the effect of increasing the spin–orbit scattering is clearly illustrated. The magnetoconductivity gradually changes from positive to negative as the strength of the spin–orbit scattering is increased.

The behaviour of the spin–orbit scattering rate with Au concentration is shown in figure 4. τ_{so}^{-1} initially increases monotonically with Au content but tends to saturate

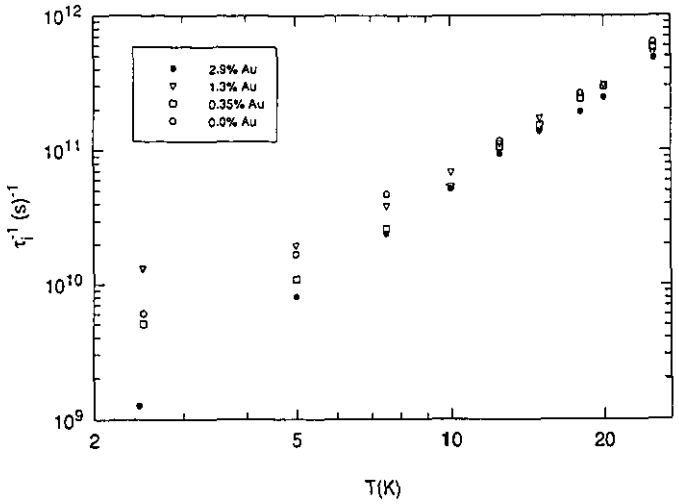

Figure 2. Inelastic scattering rate of $(Ca_{80}Al_{20})_{100-x}$ Au_x.

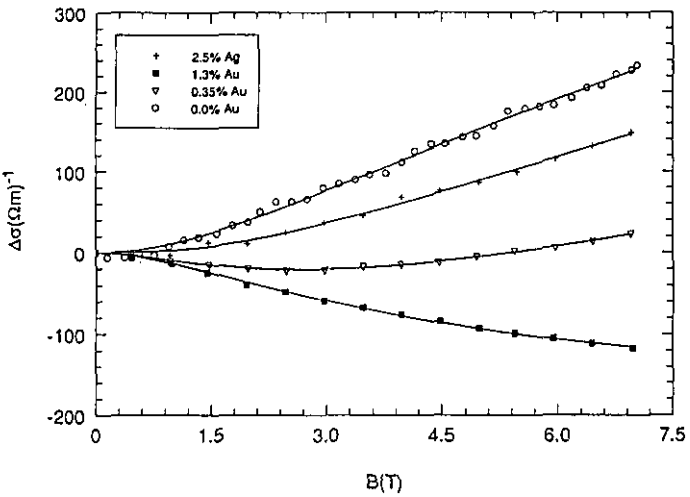

Figure 3. Magnetoconductivity of $(Ca_{80}Al_{20})_{100-x}$ (Au, Ag)$_x$ at 18 K.

at about 3% Au with a value of 10^{12} s^{-1}. Richter *et al* [4] also found a similar saturation of the spin–orbit scattering rate in their work on MgCu(Au) alloys. A possible explanation for the saturation is that as the Au concentration is increased, the distance between gold atoms approaches that of the elastic scattering mean free path. QIEs arise because of the interference between electron partial waves as they transverse self-intersecting paths in opposite senses. In order for the QIE to take effect and be affected by spin–orbit scattering, there have to be many elastic scatterings within the self-intersecting path over the time scale of the τ_{so}. Thus as τ_{so} approaches

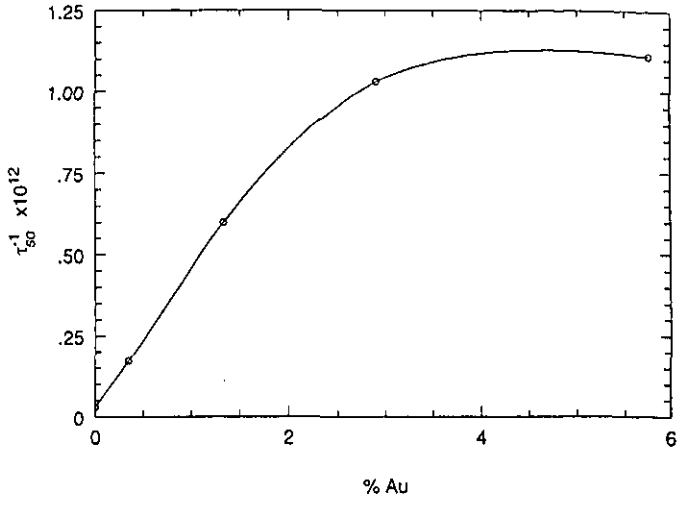

Figure 4. Spin–orbit scattering rate as a function of Au concentration in $(Ca_{80}Al_{20})_{100-x}(Au)_x$.

τ_e, the elastic scattering time, the marginal effectiveness of the spin–orbit scattering in affecting the QIE is reduced. As τ_{SO}^{-1} increases the maximum average radius of the self-intersecting paths *un*affected by spin–orbit scattering is reduced. The limit of this reduction occurs when the radius approaches the value of the elastic mean free path. This average radius is approximately $(D\tau_{so})^{1/2}$, which when τ_{so} saturates is about 50 Å.

Hickey *et al* [15] argued that the spin–orbit scattering rate is related to the atomic number Z by $\tau_{so}^{-1} \propto Z^8$. They argued that while the skew scattering spin–orbit scattering rate is proportional to Z^4 this is only first order in the spin–orbit interaction while the spin-flip spin–orbit scattering is second order in the spin–orbit interaction parameter. This Z^8 dependence is a very simplistic idea. However, we might expect there to be a correlation between this dependence and the measured ratio of scattering rates, particularly for this simple system. This dependence arises from the matrix elements of the spin–orbit coupling using one-electron hydrogenic orbitals and gives a measure of the atomic spin–orbit splitting. In fact these scale [16] as (Z^4/n^3) where n is the principal quantum number. Thus we ought to expect the spin–orbit scattering rates to scale as Z^8/n^6. Therefore for Au and Ag with Z values of 79 and 47 respectively and n of 5 and 4 (assuming it is the 5p and 4p orbitals that we should consider), $(Z_{AG}/Z_{Au})^8(n_{Au}/n_{Ag})^6 = 0.06$. From our measurements, the ratio of the rate of increase of the spin–orbit scattering rate for Ag and Au doped alloys is 0.05 ∓ 0.01.

Figures 5(*a*), (*b*) and (*c*) show the individual contributions from the QIE and EIE to the total magnetoconductivity of $Ca_{80}Al_{20}$ and $(Ca_{80}Al_{20})_{99.65}Au_{0.35}$ at $T = 2.5$ and 18 K. The contribution from the EIE is always negative and is significant only at low temperatures ($T < 10.0$ K) and high magnetic fields ($B > 3$ T). It is clear from the figures that spin–orbit scattering reduces the EIE contribution and it is in fact completely destroyed by strong spin–orbit scattering. This is an important

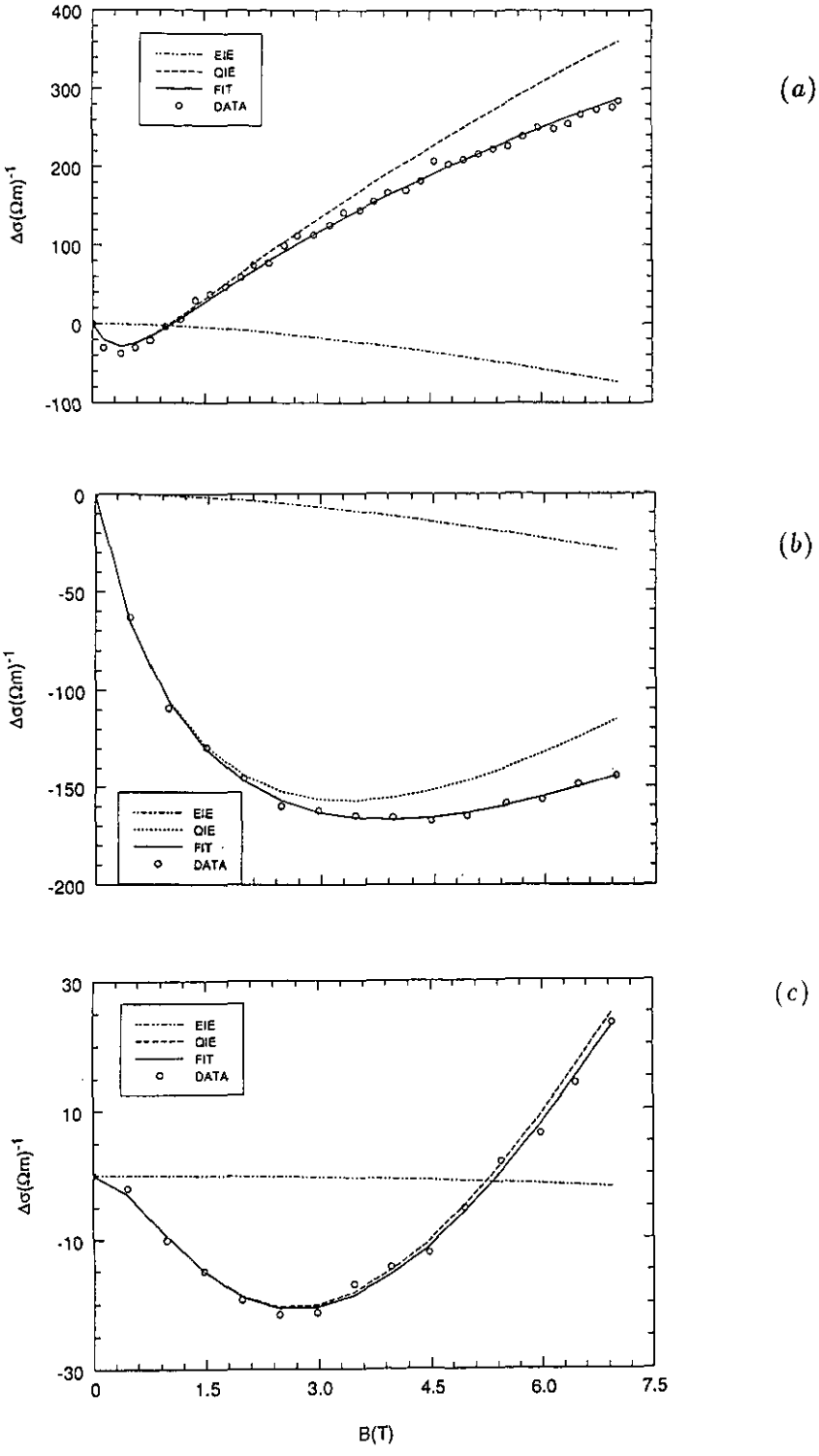

Figure 5. QIE and EIE contributions to the total magnetoconductivity in (*a*) $Ca_{80}Al_{20}$ at 2.5 K, (*b*) $(Ca_{80}Al_{20})_{99.65}Au_{0.35}$ at 2.5 K and (*c*) $(Ca_{80}Al_{20})_{99.65}Au_{0.35}$ at 18 K.

observation which has not received much attention. The reduction in the EIE contribution with increase in gold concentration is also shown from the values of the screening parameter F in table 1. The value of F decreases with increasing spin–orbit scattering. Amorphous materials have smaller F values in comparison with the corresponding crystalline systems because of the reduced electronic screening when the electronic propagation becomes diffusive. But as the spin–orbit scattering is increased the value of F is *apparently* reduced even more. In fact this reduction in F is an artifact of the fitting procedure and merely illustrates the fact that spin–orbit scattering destroys the EIE contribution to the magnetoconductivity. In the highest Au content alloys, the EIE contribution is totally absent ($F \equiv 0$).

There have been theoretical arguments that spin–orbit scattering should reduce the EIE [17, 18]. Altshuler *et al* [18] showed that in the limit of strong spin–orbit scattering the EIE contribution to the magnetoconductivity is destroyed. This is related to the fact that the dephasing time for the electron–electron interaction in a field is due to the Zeeman splitting energy difference between the spin up and spin down interacting electrons. The spin-mixing effect of the spin–orbit interaction shortens this dephasing time and renders the EIE independent of magnetic field, for strong spin-mixing.

In figures 6(*a*), (*b*) and (*c*) we show the magnetoconductivity of $(Ca_{60}Al_{40})_{100-x}Au_x$. Although the resistivity of this series is much greater than for the $(Ca_{80}Al_{20})_{100-x}Au_x$ series, the magnetoconductivity is still very similar to that of the $(Ca_{80}Al_{20})_{100-x}Au_x$ series. The various characteristic parameters are shown in table 1. We can see that the inelastic scattering is not affected by Au and that the EIEs are similarly reduced by the presence of spin–orbit scattering.

Although τ_{so} was a free parameter in the fitting procedure, it is important to note that its value for a particular alloy is independent of temperature as shown in table 2. Hickey *et al* [19] reported a slight temperature dependence in the spin–orbit scattering which is difficult to account for. However, we believe that this was because Hickey *et al* had overestimated the EIE contribution at low temperatures which in strong spin–orbit scattering alloys is probably zero.

Table 2. Scattering times for $(Ca_{80}Al_{20})_{99.65}Au_{0.35}$.

T (K)	2.5	5.0	7.5	10.5	12.5	15.0	18.0	20.0	25.0
τ_i (ns)	198.6	91.5	38.0	18.7	9.5	6.6	4.1	3.3	1.7
τ_{so} (ns)	5.6	5.6	5.7	5.7	5.6	5.8	5.8	5.4	6.0

We have also measured the temperature dependence of conductivity. However the results have proved to be much more complicated and will be presented in a separate publication.

5. Conclusion

The behaviour of the magnetoconductivity of $(Ca_{80}Al_{20})_{100-x}(Au, Ag, Cu)_x$ and $(Ca_{60}Al_{40})_{100-x}Au_x$ over the whole range of spin–orbit scattering has been illustrated and it has been shown that for a complete description a combination of the QIE and EIE is required; this is particularly true at the lowest temperatures. The change in

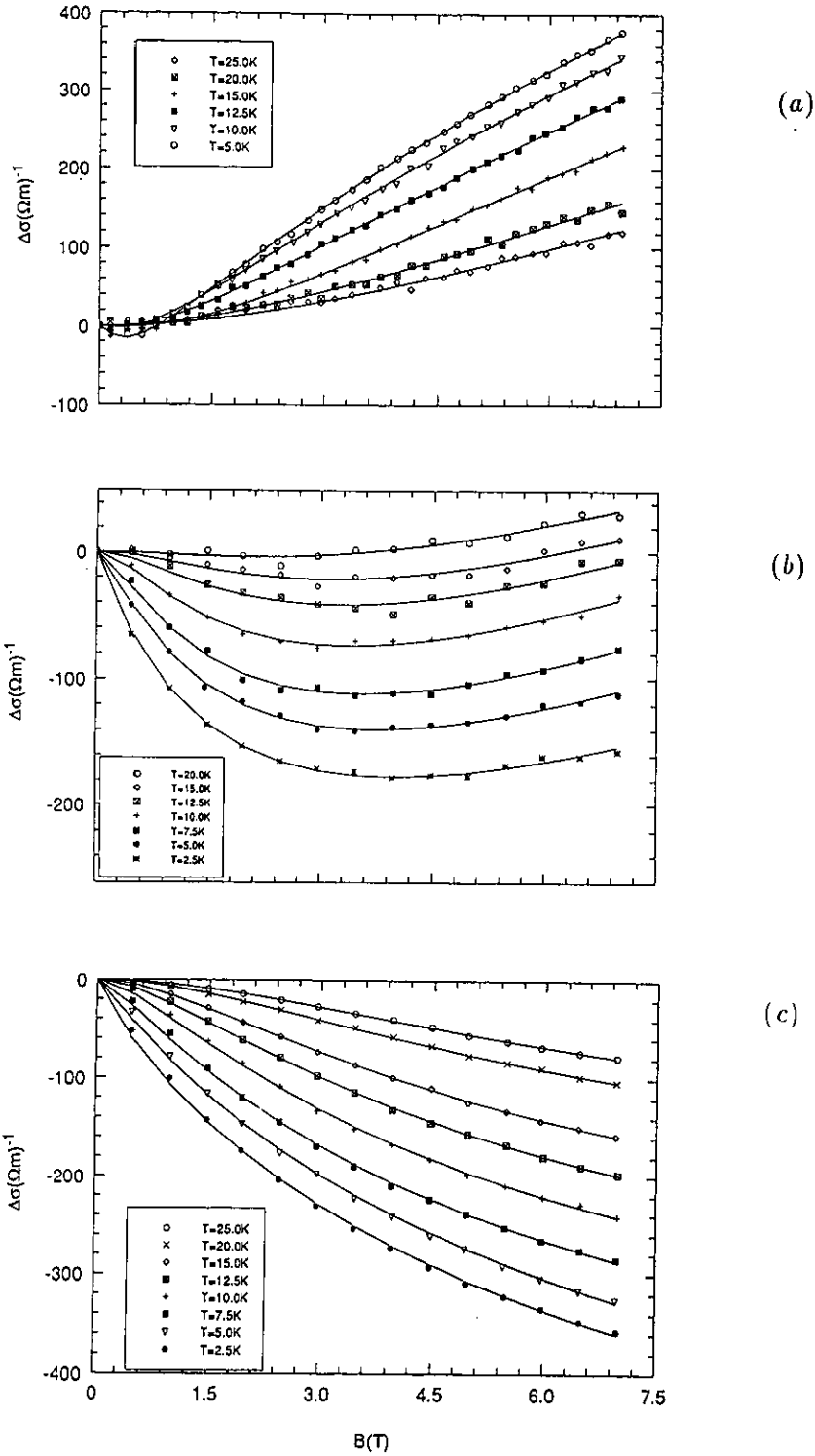

Figure 6. Magnetoconductivity of $(Ca_{60}Al_{40})_{100-x}$ Au_x for (*a*) $x = 0$, (*c*) $x = 0.2$ and (*c*) $x = 0.5$.

sign of the magnetoconductivity is predominantly due to the QIE in the presence of spin–orbit scattering. The contribution from the EIE is always negative and becomes significant at low temperatures and high magnetic field but only in the presence of weak spin–orbit scattering. There is a complete destruction of the EIE by strong spin–orbit scattering arising from the spin-mixing effect of the spin–orbit scattering.

We have shown that spin–orbit scattering due to Au and Ag is consistent with simple ideas of the dependence of the spin–orbit interaction on atomic parameters. We have also seen that the spin–orbit scattering rate appears to saturate at about 10^{12} s^{-1} because of the reduction in the marginal effectiveness of the spin–orbit scattering as τ_{so} approaches τ_e.

Acknowledgments

We would like to acknowledge the many useful discussions with Bryan Hickey and Jim Morgan. We also are grateful to Mike Walker for his help in sample preparation. This work is supported by the British Council and the University of Zambia.

References

[1] Howson M A and Gallagher B L 1988 *Phys. Rep.* **170** 265
[2] Sahnoune A and Strom-Olsen J O 1989 *Phys. Rev.* B **39** 7561
[3] Lindquist P, Rapp O, Sahnoune A and Strom-Olsen J O 1990 *Phys. Rev.* B **41** 3841
[4] Richter R, Baxter D and Strom-Olsen J O 1988 *Phys. Rev.* B **38** 10421
[5] Dugdale J S 1987 *Contemp. Phys.* **28** 547
[6] Bergmann G 1987 *Phys. Rev.* B **35** 4205
[7] Howson M A, Hickey B J and Morgan G J 1988 *Phys. Rev.* B **38** 5267
[8] Fukuyama H and Hoshino K 1981 *J. Phys. Soc. Japan* **50** 2131
[9] Baxter D, Richter R, Trudeau M L, Cochrane R W and Strom-Olsen J O 1989 *J. Physique* **50** 1673
[10] Lee P A and Ramakrishnan T V 1982 *Phys. Rev.* B **26** 4009
[11] Isawa Y and Fukuyama H 1984 *J. Phys. Soc. Japan* **53** 1415
[12] Ousset J C, Askenazy S, Rakoto H and Broto J M 1985 *J. Physique* **46** 2145
[13] Mizutani U and Matsuda T 1983 *J. Phys. F: Met. Phys.* **13** 2115
[14] Howson M A, Paja A, Morgan G J and Walker M J 1988 *Z. Phys. Chem.* **157** 693
[15] Hickey B J, Greig D and Howson M A 1986 *J. Phys. F: Met. Phys.* **16** L13
[16] Herman F and Skillman S 1963 *Atomic Structure Calculations* (Englewoods Cliffs, NJ: Prentice Hall)
[17] Millis A J and Lee P A 1984 *Phys. Rev.* B **30** 6170
[18] Altshuler B L, Aronov A G and Zuzin A Y 1982 *Solid State Commun.* **44** 137
[19] Hickey B J, Greig D and Howson M A 1987 *Phys. Rev.* B **36** 3074